Published OnlineFirst November 9, 2021; DOI: 10.1158/0008-5472.CAN-21-3360

HER3 Is an Actionable Target in Advanced Prostate Cancer

Veronica Gil[1], Susana Miranda[1], Ruth Riisnaes[1,2], Bora Gurel[1], Mariantonietta D'Ambrosio[3], Alessandro Vasciaveo[4], Mateus Crespo[1,2], Ana Ferreira[1], Daniela Brina[3], Martina Troiani[3], Adam Sharp[1,2], Beshara Sheehan[1], Rossitza Christova[1], George Seed[1], Ines Figueiredo[1], Maryou Lambros[1], David Dolling[1], Jan Rekowski[1], Abdullah Alajati[3], Matthew Clarke[1], Rita Pereira[1], Penny Flohr[1], Gemma Fowler[1], Gunther Boysen[1], Semini Sumanasuriya[1,2], Diletta Bianchini[1,2], Pasquale Rescigno[1,2], Caterina Aversa[1,2], Nina Tunariu[1,2], Christina Guo[1,2], Alec Paschalis[1,2], Claudia Bertan[1], Lorenzo Buroni[1], Jian Ning[1], Suzanne Carreira[1], Paul Workman[1], Amanda Swain[1], Andrea Califano[4], Michael M. Shen[4], Andrea Alimonti[3], Antje Neeb[1], PCF/SU2C International Prostate Cancer Dream Team, Jonathan Welti[1], Wei Yuan[1], and Johann de Bono[1,2]

ABSTRACT

It has been recognized for decades that ERBB signaling is important in prostate cancer, but targeting ERBB receptors as a therapeutic strategy for prostate cancer has been ineffective clinically. However, we show here that membranous HER3 protein is commonly highly expressed in lethal prostate cancer, associating with reduced time to castration resistance (CR) and survival. Multiplex immunofluorescence indicated that the HER3 ligand NRG1 is detectable primarily in tumor-infiltrating myelomonocytic cells in human prostate cancer; this observation was confirmed using single-cell RNA sequencing of human prostate cancer biopsies and murine transgenic prostate cancer models. In castration-resistant prostate cancer (CRPC) patient-derived xenograft organoids with high HER3 expression as well as mouse prostate cancer organoids, recombinant NRG1 enhanced proliferation and survival. Supernatant from murine bone marrow–derived macrophages and myeloid-derived suppressor cells promoted murine prostate cancer organoid growth *in vitro*, which could be reversed by a neutralizing anti-NRG1 antibody and ERBB inhibition. Targeting HER3, especially with the HER3-directed antibody–drug conjugate U3-1402, exhibited antitumor activity against HER3-expressing prostate cancer. Overall, these data indicate that HER3 is commonly overexpressed in lethal prostate cancer and can be activated by NRG1 secreted by myelomonocytic cells in the tumor microenvironment, supporting HER3-targeted therapeutic strategies for treating HER3-expressing advanced CRPC.

Significance: HER3 is an actionable target in prostate cancer, especially with anti-HER3 immunoconjugates, and targeting HER3 warrants clinical evaluation in prospective trials.

Introduction

Prostate cancer remains one of the commonest male malignancies, and a leading cause of male cancer mortality with increasing global incidence (1). Genomic studies have demonstrated that prostate cancer is a highly heterogeneous group of diseases, most of which are addicted to oncogenic androgen receptor (AR) signaling (2, 3). Prostate cancers usually initially respond to androgen deprivation therapy (ADT), but, if not cured by radical local treatment, clinical progression to metastatic castration-resistant prostate cancer (CRPC) invariably occurs. Persistent AR signaling from constitutively active AR splice variant expression (4), AR aberrations, as well as AR enhancer activity and AR cofactor function contribute to treatment resistance (5). Other pathways commonly aberrant in prostate cancer include PI3K/AKT and MEK/ERK signaling, loss of RB1 function, cell-cycle aberrations, and hijacked WNT signaling (3).

For decades, it has been recognized that ERBB signaling is implicated in CRPC (6), but clinical trials of ERBB-targeting drugs including studies of pertuzumab-targeting HER2/HER3 heterodimerization, and the small-molecule ERBB inhibitor afatinib, in combination with ADT, failed to demonstrate antitumor activity (7, 8). Unlike breast cancer (9), genomic aberrations in ERBB/HER genes are uncommon in prostate cancer (10). Consequently, the clinical evaluation of ERBB/HER receptor targeting for prostate cancer has been largely abandoned, despite the plethora of anticancer drugs targeting these receptors for the treatment of other cancers, including immunoconjugates targeting HER2 and HER3 (11–13). We elected to reinvestigate ERBB receptors in endocrine treatment-resistant lethal prostate cancer, hypothesizing that targeting ERBB receptors merits further evaluation in CRPC.

[1]The Institute of Cancer Research, London, United Kingdom. [2]The Royal Marsden Hospital, London, United Kingdom. [3]Institute of Oncology Research, Università della Svizzera Italiana, Bellinzona, Switzerland. [4]Columbia University College of Physicians and Surgeons, New York, New York.

Note: Supplementary data for this article are available at Cancer Research Online (http://cancerres.aacrjournals.org/).

V. Gil and S. Miranda contributed equally to this article.

Corresponding Author: Johann S de Bono, Clinical Studies, The Institute of Cancer Research, 15 Cotswold Road, Sutton SM2 5NG, United Kingdom. Phone: 4402-0872-24029; Fax: 4402-0864-27979; E-mail: johann.de-bono@icr.ac.uk

Cancer Res 2021;81:6207–18

doi: 10.1158/0008-5472.CAN-21-3360

Published OnlineFirst November 9, 2021; DOI: 10.1158/0008-5472.CAN-21-3360

Materials and Methods

Patient sample collection

Patients were identified from a population of men with CRPC treated at the Royal Marsden NHS Foundation Trust. All patients had given written informed consent and were enrolled in institutional protocols approved by the Royal Marsden NHS Hospital (London, United Kingdom) ethics review committee (reference no. 04/Q0801/60). Human biological samples were sourced ethically, and their research use was in accord with the terms of the informed consent provided. We analyzed 88 patients with sufficient formalin-fixed, paraffin embedded (FFPE) diagnostic (archival) castration-sensitive prostate cancer (CSPC) biopsies; 51 of these 88 patients had sufficient matching FFPE CRPC biopsies (Supplementary Fig. S1; Supplementary Table S1). All CSPC biopsies demonstrated adenocarcinoma and were from either prostate needle biopsy ($n = 72$), transurethral resection of the prostate (TURP; $n = 6$), prostatectomy ($n = 4$), or alternative sites ($n = 6$). CRPC tissue was obtained from metastatic biopsies of bone ($n = 25$), lymph node ($n = 19$), soft tissue ($n = 3$), liver ($n = 2$), and TURP ($n = 2$). All tissue blocks were freshly sectioned and only considered for IHC analyses if adequate material was present (≥50 tumor cells). Demographic and clinical data for each patient were retrospectively collected independently by A. Sharp and S. Sumanasuriya from the hospital electronic patient record system.

IHC

Tissue blocks were sectioned and only considered for analyses if adequate material was present. Protein expression was determined via IHC on 3- to 4-μm thick FFPE sections and assessed by a prostate cancer pathologist (B. Gurel) blinded to the clinical data. All cases were subsequently imaged at high resolution and scored with image analysis software. More details on the IHC assays used are available in the Supplementary Materials and Methods and Supplementary Table S2.

Multicolor immunofluorescence panel for NRG1, CD11b, CD68, and DAPI

Multiplex tissue immunofluorescence (IF) staining for NRG1, CD11b, and CD68 was performed on the Bond RX automated staining platform (Leica Biosystems) with the Opal 7-Color Automation IHC Kit (NEL821001KT, Akoya Biosciences) according to the manufacturer's instructions. IF signals for NRG1, CD11b, and CD68 were visualized using TSA dyes 570, 520, and 650 respectively, and counterstained with spectral DAPI. After staining, slides were scanned using the VS200 Microscope (Olympus) and quantification of immune cell densities expressing NRG1 was achieved with Halo v3.0 software (Indica Labs). More details on the IF assay is available in Supplementary Table S2.

Genomic characterization and mutation analysis

Patient tumor samples were analyzed as described previously (14). Briefly FFPE DNA samples were extracted with the FFPE tissue DNA kit (Qiagen), libraries were constructed for targeted sequencing using a 113 genes custom-designed panel (Generead V2, Qiagen) and then sequenced on an Illumina MiSeq with a 300 cycles V2 reagent (2 × 150). FastQ files were generated and analyzed through the Qiagen Web portal: https://geneglobe.qiagen.com/us/analyze. Where mutation data were available, for either CSPC or CRPC ($n = 41$), patients were grouped into DNA damage repair (DDR) Yes/No based on the evidence of DDR alterations. Association with membranous HER3 (mHER3) optical density (OD) was analyzed using Mann–Whitney, nonparametric, two-tailed test.

RNA sequencing

Patient-derived xenograft (PDX) and organoid RNA quality was analyzed using Agilent RNA ScreenTape assay (Agilent). A total of 500 ng of RNA from each PDX sample was used for library preparation using the NEBNext rRNA Depletion Kit followed by NEBNext Ultra II directional RNA assay kit as per manufacturers protocol (New England Biolabs). Library quality was confirmed using the Agilent High sensitivity D1000 ScreenTape Assay (Agilent). The libraries were quantified and normalized by qPCR using Generead Library Quant Kit (Qiagen). Library clustering and sequencing were performed on the Illumina NovaSeq 6000. The libraries were run across two lanes of an Illumina NovaSeq S2 flowcell using 150 bp pair-end v1 Kit and eight bp dual indexes. Base calling and quality scoring were performed using Real-Time Analysis (version v3.4.4) and FASTQ file generation and de-multiplexing using Illumina bcl2fastq2 (version 2.20).

Development of lethal prostate cancer PDX CP142

CP142 PDX model was developed as previously described for CP50 (15, 16). Briefly, a metastatic lymph node biopsy from a patient with CRPC was divided and implanted subcutaneously into an intact non-obese diabetic (NOD) scid gamma (NSG) (NOD.Cg-*Prkdcscid Il2rgtm1WjI*/SzJ) between 7–8 weeks of age male mice (termed CP142). Tumor growth was observed 6 months after implantation. Passaging of tumors was performed by implanting tumor fragments of 3 × 3 × 3 mm subcutaneously into male NSG mice. To generate castrate (C) lines termed CP142C, tumors that had been passaged four times were castrated when they reached 300 to 400 mm^3 and were harvested when they reached a size of around 1,200 mm^3. Subsequent passages were done in castrated mice. All experimental protocols were monitored and approved by The Institute of Cancer Research Animal Welfare and Ethical Review Body, in compliance with guidelines specified by the UK Home Office Animals (Scientific Procedures) Act 1986 and the United Kingdom National Cancer Research Institute guidelines for the welfare of animals in cancer research (17).

Organoid culture (patient-derived organoids)

Fresh PDX tumors from patients with CRPC were collected and immediately placed into biopsy transport media with additional ROCK inhibitor Y27632 at 10 μmol/L (S1049, Selleckchem). Tissue was mechanically dissociated to generate a single-cell suspension. Cells were embedded into extracellular matrix containing mitogens and niche factors to generate organoids as described previously (Supplementary Materials and Methods; Supplementary Tables S3; ref. 18).

Western blotting

Cells and PDX organoids (PDX-O) were lysed with RIPA buffer (Pierce) supplemented with protease inhibitor cocktail (Roche) and PhosStop phosphatase inhibitor mix (Roche). PDX lysate was obtained by mechanical homogenization, reconstituted in RIPA buffer. Protein extracts (20 μg) were separated on 4%–12% NuPAGE Bis-Tris gel (Invitrogen) by electrophoresis and subsequently transferred onto Immobilon-P polyvinylidene difluoride membranes of 0.45 μm pore size (Millipore). Chemiluminescence was detected on the Chemidoc Touch imaging system (Bio-Rad). Detailed antibodies in Supplementary Table S3.

RNA and DNA extraction

Organoids were collected using harvesting solution (3700-100-01, Cultrex Amsbio) into conical Eppendorf tubes and incubated on ice for 30 minutes to remove extracellular matrix then washed 1× with cold

sterile PBS and pelleted by cold spin. Extraction for RNA and DNA was performed using the *Quick* prep kits (Zymo Research) following manufacturer's protocols. PDX RNA was obtained by mechanical homogenization, reconstituted in RLT and then extraction was performed using the RNeasy plus kit following manufacturers protocol (Qiagen).

Single-cell analysis of prostate cancer patient samples

Single-cell RNA sequencing (RNA-seq) profiles from 13 prostate tumor samples were downloaded as UMI matrix from GEO: GSE141445 (19). The UMI matrix was processed using scanpy (v1.7.1; ref. 20) and Python (v3.8.4). Quality control was performed retaining cells with more than 500 detected genes and with at least 1,500 unique reads. Cells with more than 10,000 detected genes were discarded as potentially cell doublets. Cells with genes detected only in less than five cells were also discarded. Only cells with mitochondrial gene content below 10% of total reads were retained. After quality control, 30,329 cells were retained. Next, we transformed the data using 1e6 as scaling factor, and log-normalized the resulting counts per million matrix. Data were scaled and centered for downstream analysis. Principal component analysis and K-nearest neighbor (KNN) analyses were performed using $n = 15$ neighbors, $n = 6$ principal components (PC) and euclidean distance metric. We used the elbow method to determine the number of PCs to use for downstream analysis. To identify clusters of cells that recapitulate cell populations independently from the patient sample from which they were collected, we performed batch-balanced KNN analysis using BBKNN (v1.4.1; ref. 21). We performed clustering analysis using the Leiden algorithm with resolution parameter set to 0.15 (22). This analysis identified eight clusters that were used for downstream analysis. Next, the log-transformed matrix was used as input for the SingleR algorithm to perform single-cell level automated cell-type annotation (23) in the R environment (v4.0.4). We used the Blueprint and ENCODE reference datasets, that consists of bulk RNA-seq data for pure stroma and immune cells generated by Blueprint (24) and ENCODE projects (25). For each cluster, we assigned a label based on the most common cell type inferred from the SingleR analysis, using a majority voting system. SingleR inference was not tuned, and only low granularity cell-type assignments were processed. Cell-type labeling was manually refined on the basis of differentially expressed genes computed using the Wilcoxon test, by comparing each cluster against all the others. We used the Bonferroni method to correct for multiple hypothesis testing. We used the Uniform Manifold Approximation and Projection (UMAP) to display cells on a two-dimensional space (26, 27).

Conditioned media collection from BM-derived myeloid-derived suppressor cells and macrophages

Bone marrow–derived cells (BMDC) were collected and flushed from long bones of C57BL/6N mice and cultured with specific cytokines. For macrophage differentiation, BMDC were cultured in non-adherent cell culture 6-well plates (4×10^6 cells/well) in Iscove's modified Dulbecco's medium supplemented with 10% heat-inactivated FCS, 5% penicillin/streptomycin (P/S), and 10 ng/mL MCSF for 4 days (28). At day 4, 70% of the media was removed and organoid media (without additional rhEGF) was freshly added (18). After 48 hours, macrophage conditioned media (M-CM) was collected and filtered with a 0.22 μm filter. For myeloid-derived suppressor cells (MDSC), BMDC were cultured in 6-well culture plates at 1.5×10^6 cells/well in RPMI supplemented with 10% heat-inactivated FCS, 5% P/S, and 40 ng/mL of IL6 and GMCSF for 4 days (29). Differentiated BM cells were then collected and reseeded at 3×10^6 cells/well in 70% of organoid media (without additional rhEGF) and 30% of original media. After 48 hours, the MDSC-CM was collected and filtered with a 0.22 μm cell strainer. The CMs were used to treat mouse prostate cancer organoids. Organoids were obtained from the prostates of 10-week-old $Pten^{-/-};Trp53^{-/-}$ transgenic mice as described previously (18). Mouse PC organoids were digested with TrypLE (12605-010, Life Technologies) to obtain single-cell suspensions seeded in 96-well plates (1,000 cells/well). After 2–3 days, organoids were treated with rhNRG1 at 100 ng/mL (100-03, Peprotech) alone or in combination with M-CM or MDSC-CM (without rhEGF). After 5 days, proliferation was assessed using CellTiter-Glo 3D Cell Viability Assay (G9681, Promega) according to manufacturer's instructions.

In vivo cell growth inhibitory activity

Tumor-bearing mice were intravenously administered U3-1402 (10 mg/kg), IgG-ADC (MAAA-9289, 10 mg/kg), anti-HER3 antibody patritumab (U3-1287, 10 mg/kg) and 10 mmol/L acetate buffer-5% sorbitol-pH 5.5 as vehicle control for a total five weekly doses (CP50). A subgroup of mice ($n = 6$) treated with U3-1402 were monitored for tumor regrowth for upto 60 days. Total weekly dosing for CP142 model was three. Tumor growth measurements were taken every 2–3 days and grouped by 5-day intervals. Experiment was terminated and samples were collected 7 days after the last dose. Each point represents the mean tumor volume and SEM ($n = 6$–10) per arm of the study. Statistical significance was analyzed using ANOVA with Dunnett multiple comparisons.

Statistical analyses

HER2 and HER3 protein levels were reported as median values with interquartile ranges (IQR). For paired, same patient, CSPC and CRPC expression studies the Wilcoxon matched-pair rank test was used to compare differences in protein (mHER3 and mHER2) expression levels. Time to CRPC was defined as the time from diagnosis (date of diagnostic biopsy unless clinical diagnosis was recorded as >1 month prior to biopsy) to documented progression (radiological, PSA, or change of treatment) on luteinizing hormone-releasing hormone (LHRH) agonist alone or with anti-androgen if started before/or with LHRH agonist. Overall survival (OS) was defined as time from diagnosis to date of death (73 patients) or last follow-up/contact (15 patients; data cutoff 07/02/2019). Patient's outcomes were compared by mHER3 OD at diagnosis (< or ≥ median OD), median OS and time to CRPC were estimated using the Kaplan–Meier method. Statistical analysis of *in vivo* and *in vitro* studies was performed using ANOVA for all arms of the study with Dunnett multiple comparisons correction test and Sidak or Bonferroni corrections where applicable. All analyses were conducted, and graphs generated, using GraphPad Prism v7.

Bioinformatic analyses

Data from CRPC transcriptomes generated by the International Stand Up To Cancer/Prostate Cancer Foundation (SU2C/PCF) Prostate Cancer Dream Team were reanalyzed (3). SU2C transcriptome and cell line transcriptome reads were aligned to the human reference genome (GRCh37/hg19) using TopHat2 (version 2.0.7).

PDX transcriptome reads were aligned to human hg19 and mouse mm9 genome. Gene expression, fragments per kilobase of transcript per million mapped reads (FPKM), was calculated using Cufflinks (30).

Published OnlineFirst November 9, 2021; DOI: 10.1158/0008-5472.CAN-21-3360

Results

HER3 is highly expressed in lethal prostate cancer and has clinical relevance

We first analyzed the transcriptomes of 159 CRPC clinical biopsies acquired by the PCF/SU2C International Prostate Cancer Dream Team (2, 3) and found that *ERBB2* and *ERBB3* mRNA were highly overexpressed (top 25% quartile), unlike *EGFR* and *ERBB4* (**Fig. 1A**); we also observed a highly significant positive correlation (Spearman $P = 8.4 \times 10^{-9}$) between *ERBB2* and *ERBB3* mRNA expression (**Fig. 1B**). The HER2 protein has no known ligand, while HER3 is activated by its high-affinity ligands NRG1 and NRG2 but generates little signaling without heterodimerization; NRG1 and NRG2 were expressed at very low levels in CRPC biopsy RNA-seq (Supplementary Fig. S1A). To further explore these findings, we optimized IHC assays for HER2 and HER3 (Supplementary Fig. S1B) and established a digital, quantitative, method to assess IHC HER2 and HER3 membranous (mHER2 and mHER3) staining by automated OD assessment utilizing Halo (Indica Labs) image analysis software. We demonstrated

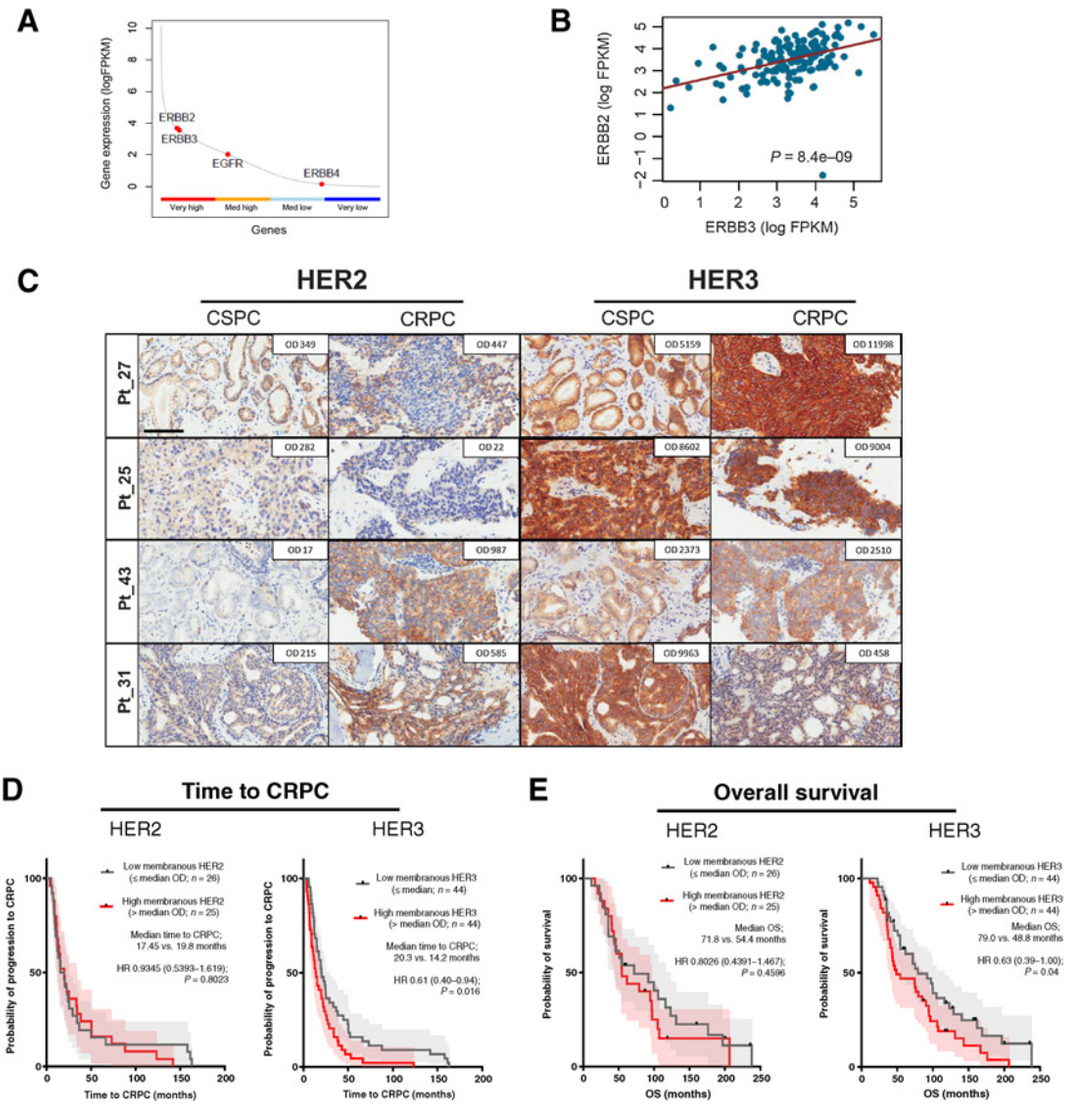

Figure 1.

HER3 expression in lethal prostate cancer has clinical relevance. **A** and **B,** Transcriptome analyses of RNA-seq data from 159 CRPC biopsies (PCF/SU2C International Prostate Cancer Dream Team) for ERBB family member expression (FPKM; **A**) and comparison of *ERBB3/HER3* (*x*-axis) and *ERBB2/HER2* (*y*-axis) mRNA expression in same patient samples showing a statistically significant positive correlation (Spearman $r = 0.4370928$; **B**). **C,** Representative IHC images of HER2 (left) and HER3 (right) protein detection in same patient CSPC and CRPC biopsies (scale bar, 100 μm), with membranous OD shown for each in top right corners. **D,** Kaplan–Meier curves for time to CRPC from diagnosis of prostate cancer for membranous HER2 expression by median OD (155.5; left) and membranous HER3 expression by median OD (2958.0; right). HER3 but not HER2 protein expression by IHC associates with time to CRPC. HR with 95% CIs and *P* values for univariate Cox survival model is shown. **E,** Kaplan–Meier curves for OS, from diagnosis of prostate cancer for membranous HER2 expression by median OD (155.5; left) and membranous HER3 expression by median OD (2958.0; right). HER3 but not HER2 protein expression by IHC associates with OS. HR with 95% CIs and *P* values for univariate Cox survival model are shown.

Published OnlineFirst November 9, 2021; DOI: 10.1158/0008-5472.CAN-21-3360

a robust correlation between a visually generated score, by a pathologist, and automated OD scores from these tumor samples by automated OD assessment (Spearman $r = 0.86$; $P < 0.0001$; Supplementary Fig. S1C). Using these assays, we next evaluated HER2 and HER3 protein expression in metastatic prostate cancer samples (**Fig. 1C**), studying treatment-naïve/CSPC biopsies from 88 men; for 51 of these men, we had matching, same patient, CRPC biopsies (Supplementary Fig. S1D; Supplementary Table S1). Membranous HER2 and HER3 proteins were detectable in both CSPC and CRPC biopsies, with HER3 being very highly expressed in many tumors (**Fig. 1C**). There was a significant correlation observed between HER2 and HER3 IHC expression at CSPC (Supplementary Fig. S1E).

To investigate the clinical significance of mHER3 expression in prostate cancer, we next evaluated these CSPC biopsies from 88 men; the median OD for mHER3 expression at diagnosis in 88 CSPC biopsies was 2,958.0 (IQR, 1643.0–5,170.0); prostate cancer with high mHER3 expression (> median OD; $n = 44$) had a significantly shorter median time to CRPC [20.3 vs. 14.2 months; HR, 0.61; 95% confidence interval (CI), 0.40–0.94; $P = 0.016$] and worse OS (79.0 vs. 48.8 months; HR, 0.63; 95% CI, 0.39–1.00; $P = 0.04$) compared with CSPC with low mHER3 (≤ median; $n = 44$; **Fig. 1D** and **E**). mHER2 staining did not associate with outcome. Overall, these data suggest that HER3 expression in lethal prostate cancer has clinical relevance.

We also studied matched, same patient, biopsies ($n = 51$) for mHER2 and mHER3 expression; mHER2 protein expression was low but increased from treatment-naïve CSPC (median OD; IQR: OD 155.5; 62.2–307.6) to CRPC (median OD; IQR: OD 404.4; 46.4–596.9). mHER3 expression was very high in both CSPC and CRPC biopsies, but surprisingly decreased slightly although remaining high ($P = 0.007$) from CSPC (median and IQR in CSPC: OD 2373.0; 879.9–5225.0) to CRPC (median and IQR in CRPC: OD 980.4; 259.7–2,540.0; Supplementary Fig. S1F). This may be explained by the timing of our CRPC biopsy acquisition, these being taken after discontinuation of the next-generation hormonal agents abiraterone and enzalutamide in the face of a rising PSA; previous reports indicate that increased AR signaling upregulates the E3 ubiquitin ligase RNF41/nrdp1 (neuregulin receptor degradation protein-1) that decreases HER3 protein levels (31).

Interestingly, treatment-naïve diagnostic biopsy/CSPC mHER3 expression associated with Ki67 expression in 74 available samples (Supplementary Fig. S1G; Supplementary Table S2). IHC analysis in diagnostic biopsies showed no correlation between mHER3 OD and ERG expression (by IHC), PTEN loss (by IHC; H-score <10), or DDR defects detected by next-generation sequencing in both CSPC and CRPC samples (Supplementary Fig. S1H).

HER2 and HER3 expression was detected at a much lower level in benign prostatic samples; in these, HER2 protein expression was weak, with incomplete membranous staining in a small number of glands and a very low median mHER2 OD of 8.3 (IQR, 2.7–38.4, $n = 6$). Cytoplasmic HER2 staining was likewise very weak. Similarly, mHER3 protein in benign prostatic glands was either low or absent. The median mHER3 OD in benign glands was 179.8 (IQR, 0.5–280.2, $n = 5$), with accompanying weak cytoplasmic staining (Supplementary Fig. S1I). Overall, these data suggested that HER2 and HER3 play a clinically important role in prostate cancer biology (32, 33).

HER3 is highly expressed in CRPC PDXs

We have previously described CP50, a PDX generated from a metastatic CRPC biopsy with chromosome 8 gain (MYC locus), AKT and AR amplification and ATM loss (15, 16). The CP142 PDX was developed from the lymph node biopsy of a patient with low PSA and a prostate cancer with neuroendocrine (NE) differentiation progressing on ADT, who proceeded to platinum-based chemotherapy after this biopsy (Supplementary Fig. S2A). Whole-exome sequencing of the lymph node biopsy of origin and the CP142 PDX (Supplementary Fig. S2B) revealed a common and deleterious TP53 Y220C mutation with IHC studies revealing RB1 loss and synaptophysin positivity (Supplementary Fig. S2C). After establishing CP142 in intact mice, a subset of this PDX was developed and maintained exclusively in castrate mice and designated CP142C (Supplementary Fig. S2A). We studied HER3 expression and signaling by IHC and Western blot analysis in these patient-derived CRPC models (PDXs) and showed increases in phosphorylated-HER3, AR-V7, and phosphorylated-AKT in castrated CP50 adenocarcinoma model in keeping with previous reports (**Fig. 2A** and **C**; ref. 34). Conversely, we did not observe an increase in phosphorylated-HER3 or phosphorylated-AKT by Western blot analyses in CP142, the model with NE differentiation (**Fig. 2B** and **D**), which has low HER3 protein expression.

RNA-seq of these PDXs confirmed that HER2 and HER3 mRNA were highly expressed with lower EGFR, and minimal ERBB4 expression in both the intact and castrate states, suggesting that HER2 may be the preferred HER3 dimerization partner. NRG1 and NRG2 mRNA was expressed at very low levels, both before and after castration (**Fig. 2E** and **F**) although low levels of NRG1 protein were detected, (**Fig. 2A** and **B**; Supplementary Fig. S3), especially in castrated mice bearing CP142C, suggesting possible upregulation of NRG1 expression after androgen deprivation in this model (**Fig. 2C** and **D**). Interestingly, these data also indicate posttranscriptional regulation of HER3 protein expression, with high HER3 mRNA but low HER3 protein in the model CP142. Overall, these data suggest that ligand independent, and/or ligand-dependent, HER3 heterodimerization and signaling may play an important biological role in castration resistance.

NRG1 expression in inflammatory cells in prostate cancer biopsies

Ligand-induced activation of HER3 by neuregulins plays a key role in driving proliferation in HER3-positive tumors and has been recently suggested to play a role in prostate cancer biology in a subpopulation of prostate cancer (35). To gain further insights into the potential clinical significance of this axis in prostate cancer, we studied the IHC expression of the predominant neuregulin, NRG1, utilizing a validated assay (Supplementary Fig. S3) in a cohort of prostate cancer biopsies ($n = 46$) and found that both CSPC and CRPC tumors had low NRG1 cytoplasmic staining by IHC (Supplementary Fig. S4B, left; **Fig. 3A**), similar to what was seen in our PDXs, with no discernible nuclear or membranous accentuation and little RNA*ish* positive staining (Supplementary Fig. S4A and S4B). Interestingly, there were no detectable differences between tumor cell NRG1 protein expression in CSPC and CRPC. NRG1 staining in the peritumoral stroma, however, showed greater variability based on cell type and intensity of expression. We, however, surprisingly observed NRG1 positivity in peritumoral inflammatory cells including neutrophils as well as intratumor myeloid cells with interestingly NRG1 protein levels in inflammatory cells being significantly higher in CRPC samples than those present in CSPC, suggesting that castration induces NRG1-expressing myelomonocytic cell recruitment (**Fig. 3A** and **B**). NRG1 expression was detectable in stromal fibroblasts as described previously (36), albeit at much lower intensity and sparser density in the peritumoral stroma compared with inflammatory cells. NRG1 staining intensity

Published OnlineFirst November 9, 2021; DOI: 10.1158/0008-5472.CAN-21-3360

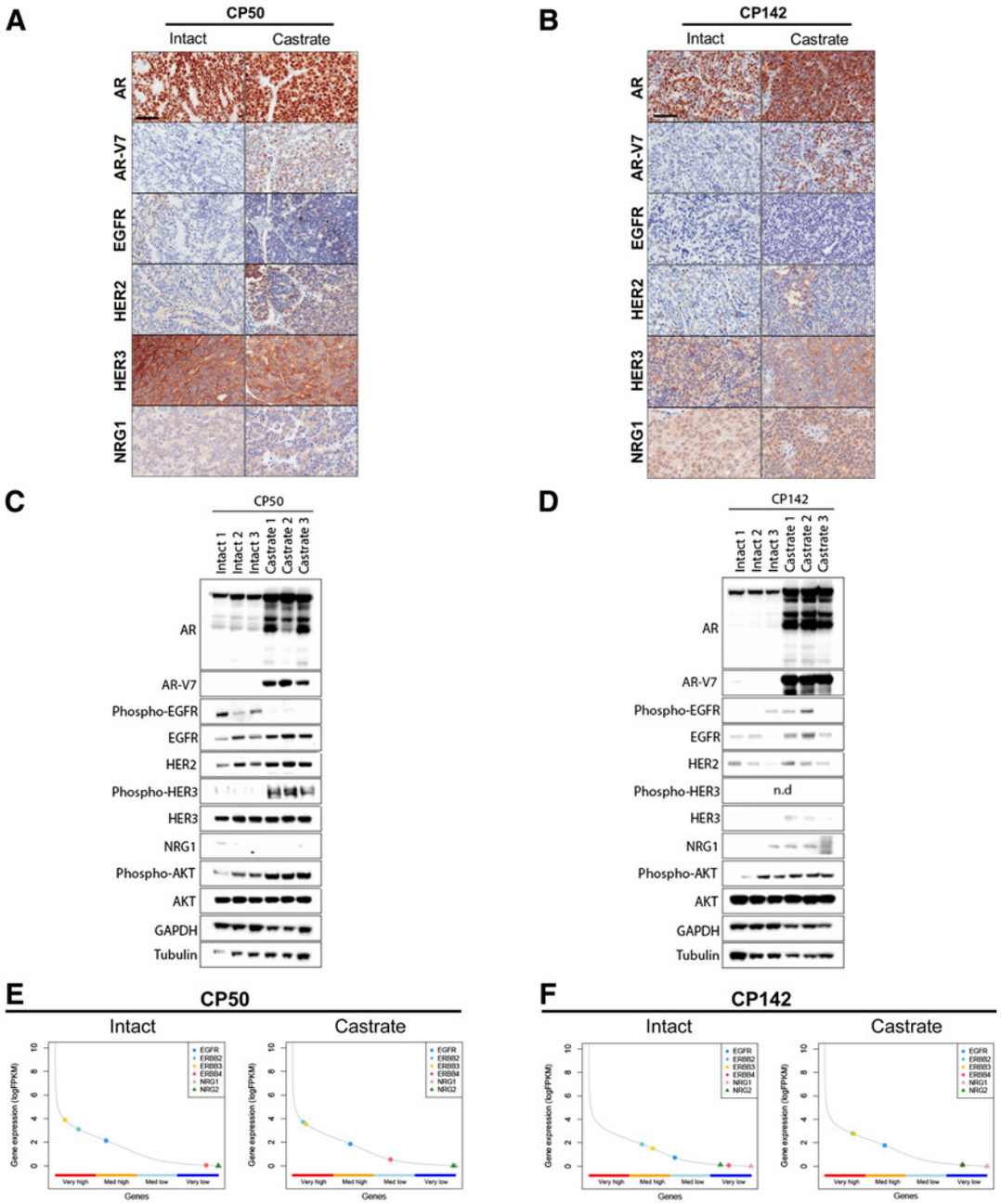

Figure 2.

Upregulation of HER3 expression in CRPC models. **A** and **B,** AR, ARv7, EGFR, HER2, HER3, and NRG1 protein expression by IHC on PDX tumor samples developed in intact and castrated mice for CP50 (**A**) and CP142 (**B**). Scale bar, 50 μm. **C** and **D,** Western blot analysis showing AR, ARv7, NRG1, and ERBB receptors expression and phospho-AKT pathway activation in same models as **A** to **B**. n.d., proteins below detection level. **E** and **F,** Transcriptome analyses of RNA-seq data on intact ($n = 3$; left) and castrate ($n = 3$; right) PDX tumor samples, for ERBB family member and NRG1 and NRG2 ligands expression (FPKM), divided into very high (upper 25% expressed genes), medium high (50%–75% expressed genes), medium low (25%–50% expressed genes), and very low (lower 25% expressed genes), in same models as **A** and **B**.

in cells in the tumor stroma was usually stronger than seen in prostate cancer (Supplementary Fig. 4B, left). Further evaluation using multicolor IF confirmed the high expression of NRG1 in CD11b-positive myelomonocytic inflammatory cells as well as CD68-expressing cells (**Fig. 3A**). Consistent with paracrine secretion of NRG1 by this inflammatory component, we performed Western blot analyses of NRG1 utilizing mononuclear cells from apheresis products from patients with CRPC ($n = 9$) and confirmed NRG1 expression in circulating mononuclear cells (Supplementary Fig. S4C).

Published OnlineFirst November 9, 2021; DOI: 10.1158/0008-5472.CAN-21-3360

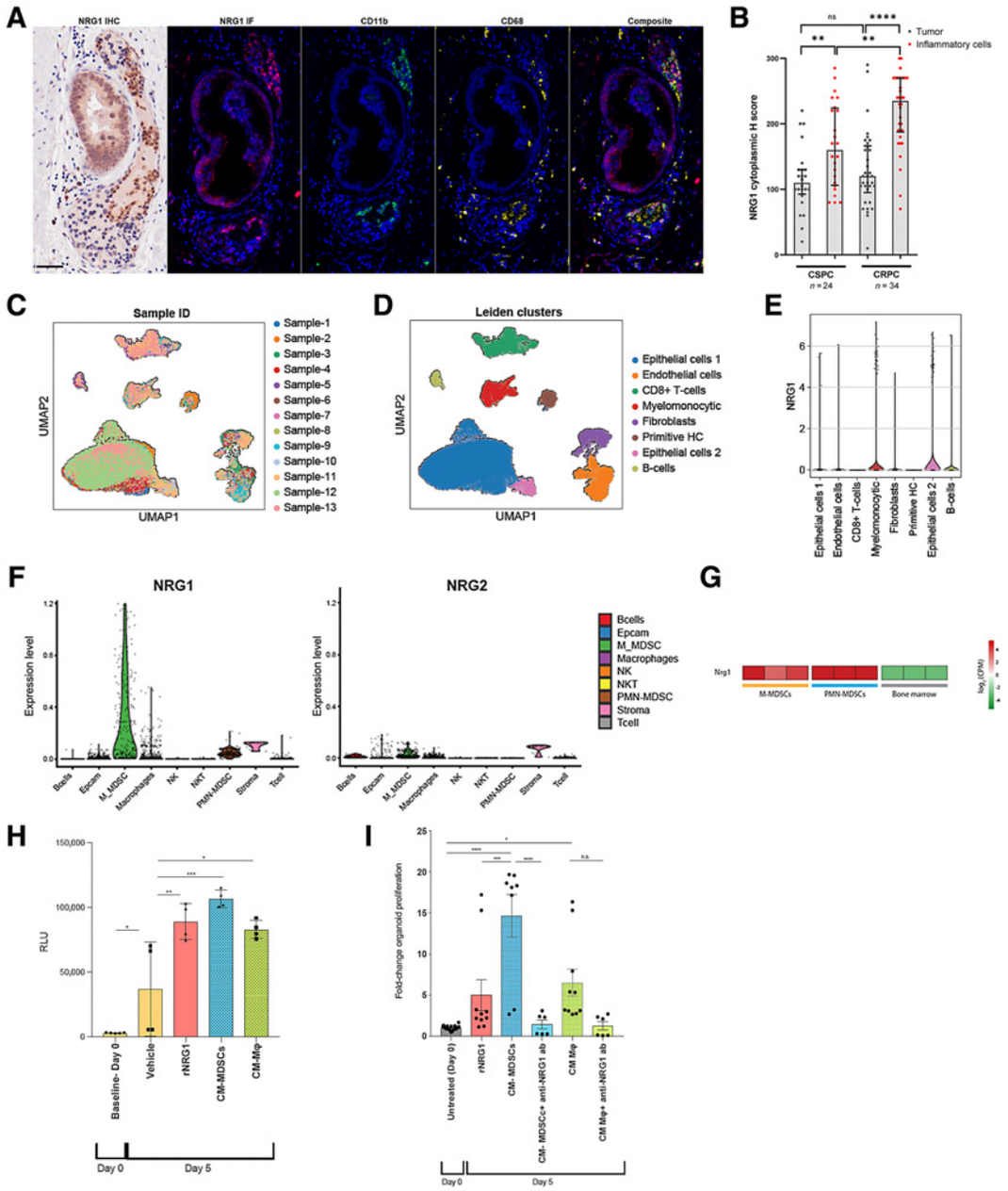

Figure 3.

NRG-activated HER3 signaling in lethal PC. **A,** Representative micrographs of prostate cancer patient samples, showing NRG1 protein expression, by IHC and IF, in CD11b (green) and CD68 (yellow) positive inflammatory cells. Scale bar, 50 μm. **B,** NRG1 protein expression, by IHC, in prostatic adenocarcinoma samples, CSPC (left; $n = 24$) and CRPC (right; $n = 34$), showing significantly higher expression in inflammatory cells (red) compared with tumor (gray; Mann–Whitney test, P values: **, $P \le 0.01$; ****, $P \le 0.0001$, median H-score, and interquartile range shown) and showing significantly higher expression in inflammatory cells present in CRPC, compared with inflammatory cells present in CSPC. No significant differences were observed between CSPC and CRPC tumor cells (Mann–Whitney test, P values: **, $P \le 0.01$; ****, $P \le 0.0001$; ns, nonsignificant). **C,** UMAP projection of 30,329 single-cell gene expression profiles from 12 primary and one lymph node metastasis tissue samples ($n = 13$) of 12 patients with prostate cancer color-coded per sample. **D,** Leiden algorithm identifies eight clusters. Clusters are color coded by SingleR-inferred cell subtype. **E,** Violin plots depicting NRG1 expression levels per assigned cell subtype. **F,** Violin plot representing frequency of immune, epithelial, and stroma cells expressing NRG1 and NRG2 subtypes from FACS sorted from murine prostate tumors Pten$^{-/-}$ followed by single-cell transcriptome analysis ($n = 2$). **G,** RNA-seq of FACS-sorted murine BM-derived MDSCs, heatmap of log-CPM values for NRG1 genes in M-MDSCs, PMN-MDSCs, and BM ($n = 3$; FDR adjusted, $P < 0.05$). **H,** Relative luminescence (RLU) as a measure for mouse prostate organoid proliferation within 5 days in conditional media generated from C57BL/6N mice BM-differentiated MDSCs and macrophages. Baseline organoid media as vehicle control with and without rNRG1 (ordinary two-way ANOVA with Tukey correction test, P values: *, $P \le 0.05$; **, $P \le 0.01$; ***, $P \le 0.001$). **I,** Experimental validation of functional NRG1 in conditional media from MDSCs and macrophages by antibody neutralization at 3 μg (Heregulin 2573; Cell Signaling Technology). Luminescence readings at 5 days (ordinary two-way ANOVA with Tukey correction test, P values: *, $P \le 0.05$; **, $P \le 0.01$; ***, $P \le 0.001$; ****, $P \le 0.0001$).

Published OnlineFirst November 9, 2021; DOI: 10.1158/0008-5472.CAN-21-3360

We next analyzed single-cell RNA-seq profiles from an independent cohort of 13 prostate tumor samples, recently published and publicly available (19), and confirmed that the highest levels of NRG1 mRNA were present in CD11b and CD68 positive clusters, with high expression also detected in a TP63 cell cluster, in keeping with basal-like tumor cell expression of NRG1 (**Fig. 3C–E**; Supplementary Fig. S4E). Overall, these data surprisingly indicate that NRG1 expression in lethal prostate cancer is primarily generated by myelomonocytic inflammatory cells.

NRG1 and myelomonocytic cells in a transgenic prostate cancer model

To unravel the role of immune cell infiltrates in paracrine NRG1 secretion, we next investigated single-cell RNA-seq data generated from prostatic tumors resected from *Pten*$^{-/-}$ transgenic mice, disaggregated into single-cell suspensions and then FACS sorted using established lineage markers. These data confirmed that myelomonocytic cells including FACS-sorted cell subtypes of monocytic-MDSCs (M-MDSC) and macrophages expressed the highest levels of *NRG1* mRNA in transgenic models while peripheral mononuclear cell MDSCs (PMN-MDSC) and stromal cells expressed lower but detectable levels of *NRG1* (**Fig. 3F**). These data also supported NRG1 as the predominant expressed cytokine over NRG2. We consistently confirmed that NRG1 RNA and protein were primarily expressed by murine BM-derived precursors including M-MDSCs, PMN-MDSCs, and macrophages by Western blot and RNA-seq analyses (**Fig. 3G**; Supplementary Fig. S4D). To study whether NRG1 secretion by myelomonocytic cells fuels prostate cancer growth, mouse prostate cancer organoids (*Pten*$^{-/-}$*Trp53*$^{-/-}$) were exposed to conditioned media from their sorted, cultured, MDSCs and macrophages (28, 29). These conditioned media significantly increased the proliferation of murine prostate cancer organoids, with this being reversed by a neutralizing anti-NRG1 antibody, suggesting that prostate cancer growth is at least in part mediated by paracrine NRG1 secretion generated by these myelomonocytic cells (**Fig. 3H** and **I**; Supplementary Table S3). Overall, these data provided further evidence that myelomonocytic inflammatory cells generate paracrine NRG1 that activates HER3 heterodimerization and signaling in prostate cancer.

HER3 activation promotes growth in patient-derived organoid models of prostate cancer

We next studied whether NRG1-mediated HER3 activation impacts the growth of human CRPC PDX-O models *in vitro* (**Fig. 4A**). We demonstrated that the addition of recombinant NRG1 (rNRG1) to these organoid cultures substantially increased cell growth in the HER3-positive model CP50, where a 2-fold increase in cell proliferation was observed, with the formation of larger and morphologically distinctive organoids comprising bigger cellular areas (Supplementary Fig. S5A; ref. 37). This effect was not observed in the HER3 low model CP142 PDX-Os. NRG1-mediated HER3 activation was demonstrated by pHER3 expression in CP50 PDX-O model by Western blot analysis (**Fig. 4A**, right) and with increasing concentrations of NRG1 *in vitro* that being reversed with anti-HER3 antibody (U3-1287 patritumab; Supplementary Fig. S5B). Overall, these data suggested that NRG1 activation of HER3 may increase prostate cancer growth in a ligand-dependent manner.

Targeting HER3 *in vitro* and *in vivo* in patient-derived models and cell lines

Targeting ERBB signaling in clinical trials has to date failed to impart patient benefit, perhaps due to feedback loops, continued AR signaling, or insufficient blockade of the entire ERBB axis (9, 10). To circumvent these challenges, we elected to study the antitumor activity of not only the anti-HER3 antibody patritumab but also of the anti-HER3 antibody–drug conjugate (ADC) U3-1402 (Daiichi Sankyo), in our prostate cancer cell lines and PDX-O models *in vitro*. This ADC (U3-1402) is in early clinical trials (NCT02204345, NCT02980341; ref. 11) and is comprised of an anti-HER3 antibody joined, via a peptide-based linker, to a topoisomerase-1-inhibitor payload (DXd), which will generate double-strand DNA breaks that can result in tumor kill (38). The antitumor activity of U3-1402 was compared with that of the parental anti-HER3 antibody (patritumab) and a control, nontargeted, IgG-ADC (MAAA-9289) conjugated to payload Dxd. Single-agent HER3 targeting by patritumab alone had antitumor activity *in vitro* in the HER3 high-expressing CP50 patient-derived model (**Fig. 4B**), but little antitumor activity against the HER3-positive prostate cancer cells lines LnCaP, LnCaP95, and 22RV1 (Supplementary Fig. S5C and S5D), perhaps indicating that the development of HER3-targeting agent requires rational combination studies targeting all active ERBB receptors as well as the AR. Patritumab also had little antitumor activity against the HER3 low CP142 model *in vitro* (**Fig. 4B**). Conversely, the anti-HER3 immunoconjugate U3-1402 had antitumor activity in the *in vitro* model CP50 (**Fig. 4B**) and the HER3-positive prostate cancer cell lines (LNCap, LNCap95, and 22Rv1) (Supplementary Fig. S5D). Interestingly, both the anti-HER3 antibody (patritumab; ref. 39) and the anti-HER3 ADC (U3-1402) had *in vitro* antitumor activity against the HER3 high PDX-O CP50, suggesting signaling inhibition in this model impacts tumor growth (**Fig. 4B**, left). Of note, some off-target antitumor activity was observed with the IgG-ADC control *in vitro* in the CP142-PDX-O model and LNCap95 cell line tested suggesting payload drug sensitivity for these tumor cells at higher doses (**Fig. 4B**; Supplementary Fig. S5D). The HER3-dependent response of U3-1402 was supported by the limited antitumor activity of the ADC observed in the HER3-low model CP142 *in vitro* (**Fig. 4B**, right; ref. 40).

We finally evaluated the *in vivo* antitumor activity of U3-1402 and patritumab in the HER3-positive and ATM-deficient CRPC PDX model CP50, which originated from a patient who had progressed through all standard-of-care therapies including docetaxel, cabazitaxel, abiraterone, and enzalutamide (16). U3-1402 demonstrated potent and sustained antitumor activity when utilizing a weekly dosing regimen at 10 mg/kg for a total of five doses (**Fig. 4C**, left). U3-1402 was effective without inducing any body weight loss or apparent toxicity in these mice. In addition, no tumor regrowth was observed for up to 60 days following the end of dosing. Patritumab demonstrated little antitumor activity in this model, suggesting that blocking HER3 alone may not have antitumor activity *in vivo* while the cytotoxin (Dxd) linked to a nonspecific antibody (MAAA-9829) also displayed minimal antitumor activity, indicating HER3-dependent targeting. We also studied the low HER3-expressing *in vivo* model CP142-PDX treated with the same dose (10 mg/kg) of U3-1402 weekly for a total of three doses and observed that U3-1402 and patritumab had minimal antitumor activity in this model (**Fig. 4C**, right) highlighting the relevance of high HER3 expression as a functional therapeutic target of U3-1402.

Discussion

There remains an urgent need to develop new therapeutic strategies to improve outcome for advanced prostate cancer (41). Twenty years ago, studies implicated HER2 signaling as a mechanism for endocrine treatment resistance in models of prostate cancer (6). This led to the

Published OnlineFirst November 9, 2021; DOI: 10.1158/0008-5472.CAN-21-3360

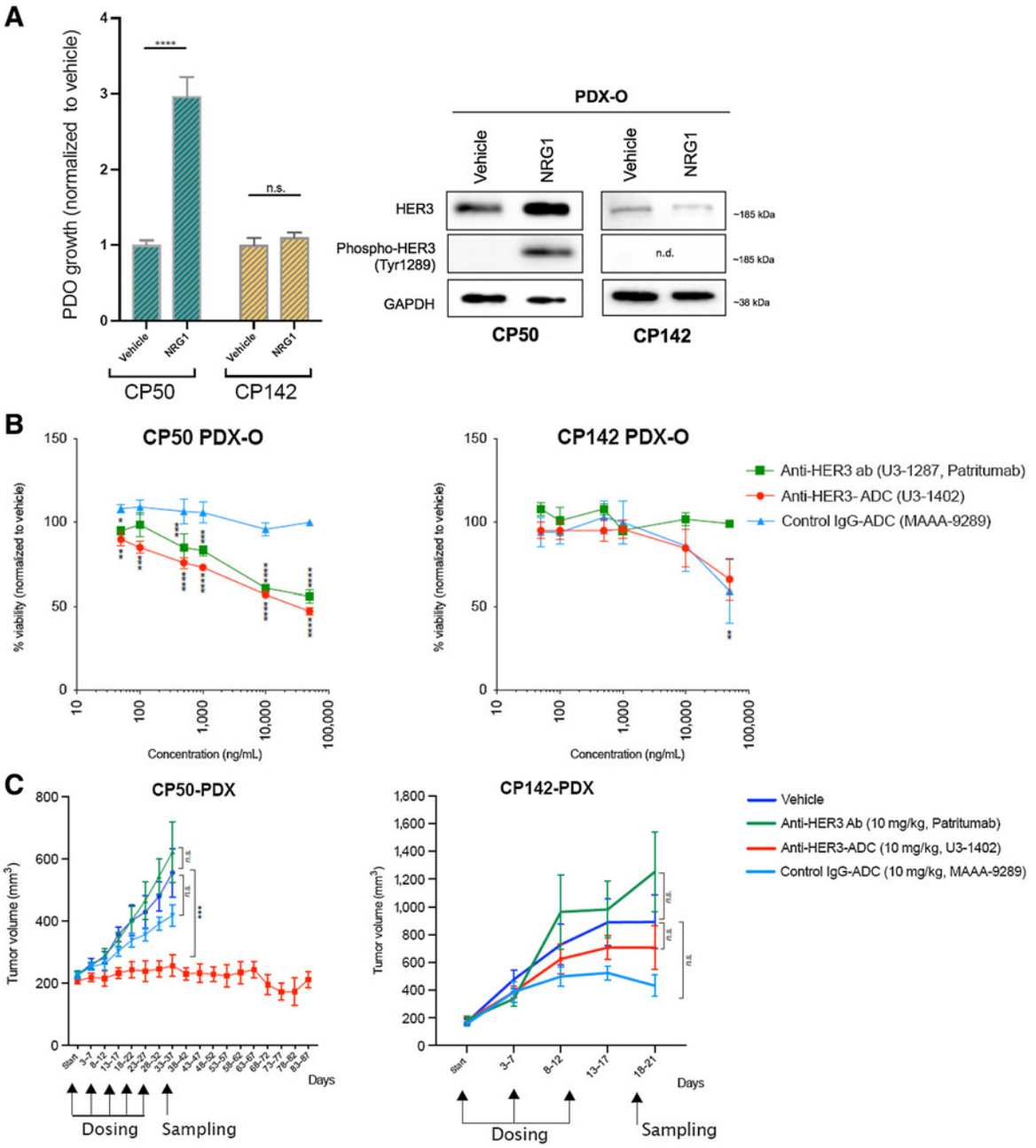

Figure 4.

Antitumor activity of anti-HER3 ADC U3-1402. **A,** Organoid proliferation normalized to untreated vehicle in PDX-O models CP50 and CP142 ($n = 3$) monitored for 7 days with and without additional rNRG1 (100 ng/mL). ANOVA with Sidak correction test was applied; *P* value: ****, $P \leq 0.0001$ (left). Immunoblots depicting phosphorylated-HER3 expression with additional rNRG1 in CP50 and CP142 PDX-O CRPC models after 16-hour treatment with human rNRG1 (100 ng/mL). GAPDH was used as loading control (right). n.d., below detection level. **B,** *In vitro* cell growth inhibitory activity of the anti-HER3 ADC U3-1402 (red line) and the anti-HER3 antibody without payload U3-1287 (patritumab; green line) in the PDX-O model CP50 (left) and CP142 (right), monitored for 7 days with endpoint assay luminescence. All results are expressed as mean ± SEM ($n = 3$). Statistical significance was analyzed using ANOVA with Dunnett multiple comparisons correction test to analyze mean difference per concentration of U3-1402 and U3-1287 (patritumab) versus IgG-ADC control (MAAA-9289; blue line), *P* values: *, $P \leq 0.05$; **, $P \leq 0.01$; ***, $P \leq 0.001$; ****, $P \leq 0.0001$. **C,** *In vivo* efficacy of the anti-HER3 ADC U3-1402 (10 mg/kg; red line) in PDX models CP50 (left) and CP142 (right); the anti-HER3 antibody without payload U3-1287 (patritumab; 10 mg/kg, green line) and IgG-ADC (MAAA-9289; 10 mg/kg, purple line) are also shown. CP50-PDX treated with U3-1402 was monitored for 5 weeks post-dosing (*P* value: ***, $P \leq 0.001$; n.s., nonsignificant) and treatment was administered weekly for a total of five times (black arrows) while CP142-PDX received a total of three weekly doses. Vehicle, 10 mmol/L acetate buffer-5% sorbitol-pH 5.5 (blue line). All results were expressed as mean ± SEM ($n = 10$) and statistical significance was analyzed using ANOVA with Dunnett multiple comparisons correction test to analyze mean difference of each treatment versus vehicle control 7 days post-treatment, corresponding to last tumor measurement.

Published OnlineFirst November 9, 2021; DOI: 10.1158/0008-5472.CAN-21-3360

conduct of multiple clinical trials for men suffering from CRPC using ERBB-targeting drugs including pertuzumab and afatinib but these demonstrated little antitumor activity as single agents (7, 8). While these trials predated the identification of continued AR signaling as a cause of castration resistance, and clinical studies with abiraterone and enzalutamide (42), they discredited targeting ERBB signaling as a therapeutic strategy for CRPC. More recent studies have implicated the NRG1/HER3 axis as playing a role in prostate cancer biology, suggesting that neuregulin is fibroblast generated (34). We now provide strong evidence to further validate HER3 as a therapeutic target for the treatment of advanced prostate cancer, demonstrating that: (i) its overexpression associates with poorer time to castration resistance and worse OS and higher Ki67; 2) confirming that androgen deprivation can increase HER3 phosphorylation in PDX models *in vivo*; (iii) the HER3 ligand NRG1 is primarily paracrine and mostly expressed by inflammatory myelomonocytic cells, increasing patient-derived model growth in HER3-expressing tumors; (iv) that while *in vitro* targeting of HER3 signaling has antitumor activity, *in vivo* targeting of HER3 signaling has minimal impact on tumor growth possibly due to the release of other paracrine factors such as IL23 by myelomonocytic cells (23); (v) but that an anti-HER3 immunoconjugate with a topoisomerase-1 inhibitor payload has impressive and durable antitumor activity against prostate cancer models expressing high (but not low) levels of HER3 with little antitumor activity from a nonspecific antibody immunoconjugate with the same payload.

HER3 is largely considered a kinase-dead receptor due to alterations of conserved residues in the catalytic domain (43), though evidence exists for HER3 autophosphorylation, indicating that this receptor may preserve some weak kinase activity (44). HER3 largely signals through heterodimerization with other ERBB receptors, although heterodimerization with noncanonical receptors has been suggested (33, 45). Interestingly, we demonstrate an increase in HER2 expression at castration resistance and also demonstrate that in patient biopsies and transgenic mouse models of prostate cancer that NRG1 is largely generated by myelomonocytic inflammatory cells, which increase with castration resistance; these have been previously demonstrated to be chemoattracted down a chemokine gradient into prostate cancer stroma after androgen deprivation and to fuel prostate cancer cell proliferation and tumor growth by secreting paracrine factors including IL23, which we have shown to upregulate AR signaling (28, 29) Unlike IL23, NRG1-activated HER3 activates AKT signaling by preferentially heterodimerizing with HER2 through HER3 phosphorylation (32, 46). Overall, this suggests that chemoattracted myelomonocytic cells can release paracrine factors that activate both AR and AKT signaling.

We also demonstrate in the studies herein that in CRPC while both HER2 and HER3 mRNAs are highly co-overexpressed, HER2 protein is expressed at much lower levels although it increases at castration resistance. We also demonstrate HER3 signaling activation in our PDX models *in vivo* upon castration. We have, however, been unable to disprove ligand-independent HER3 activation, but have demonstrated little evidence for autocrine tumor cell generation of the high-affinity HER3 neuregulin ligands NRG1 and NRG2 by IHC and RNA*ish* in adenocarcinoma although our studies suggest that NE prostate cancer cells may express NRG1. Furthermore, we could not identify any cases of NRG1 fusions/translocations in available CRPC genomic data as has been suggested for other cancers and at least one case of prostate cancer (47).

We do, however, show that in patient-derived CRPC models HER3 paracrine activation by NRG1, increases tumor growth (36). Overall, these results have led to our routine use of rNRG1 in CRPC organoid cultures to enable their longer-duration culture, which had been a major challenge (48). Our data indicate paracrine NRG1 in lethal prostate cancer is primarily generated by inflammatory cells, although some fibroblast NRG1 expression was also detected. NRG1 staining in the peritumoral stroma was observed in lymphocytes, histiocytes, and mature neutrophils. This was supported by studies of BM precursors from prostate cancer transgenic models (49).

Because HER3 activation activates PI3K/AKT activation and other signaling pathways, inhibition of myelomonocytic cell generated NRG1-induced HER3 activity is worth pursuing in clinical studies. However, it is likely that blockade of not only ERBB signaling but also of other paracrine factors released by myelomonocytic cells including IL23, which fuels AR and AR splice variant signaling through RORγ, will be required to generate tumor cell kill. Thus, we evaluated the antitumor activity of not only the anti-HER3 antibody patritumab but also of U3-1402, an anti-HER3 ADC linked to a topoisomerase-1 inhibitor exatecan derivative (Dxd); this significantly inhibited tumor growth in multiple HER3-expressing model with little antitumor activity in a HER3 low model. We acknowledge that further studies of drug combinations incorporating HER3/ERBB inhibitor combinations are warranted, such as the co-targeting of IL23/IL23R/RORγ and HER3 signaling with the absence of these data being a limitation of our studies.

In conclusion, the data herein indicate that HER3 has clinical relevance in lethal prostate cancer where it is commonly expressed, being most likely activated in CRPC by NRG1 secreted from myelomonocytic cells. We also present data indicating that HER3 merits targeting by anti-HER3 immunoconjugate therapy in clinical trials for men suffering from high HER3-expressing lethal prostate cancer and envision that these can add prostate cancer to the list of common tumors that can be treated by ERBB-targeting strategies.

Authors' Disclosures

A. Vasciaveo reports grants from U.S. Army Medical Research and Development Command (USAMRDC) during the conduct of the study. A. Sharp reports other support from Sanofi, Roche-Genentech, and Astellas Pharma outside the submitted work; and A. Sharp is an employee of The Institute of Cancer Research (ICR), which has a commercial interest in abiraterone. G. Boysen reports other support from Astellas Pharma Europe outside the submitted work. D. Bianchini reports personal fees from Pfizer and Janssen outside the submitted work. P. Rescigno reports other support from MSD Italy and AstraZeneca Italy outside the submitted work. C. Guo reports grants from United States Department of Defense, Wellcome Trust, and Prostate Cancer Foundation outside the submitted work. P. Workman reports grants from CRUK, Wellcome, Chordoma Foundation, and Mark Foundation during the conduct of the study; personal fees from Astex Therapeutics, Storm Therapeutics, Nextechinvest, CV6 Therapeutics, Black Diamond Therapeutics, Vividion Therapeutics; grants from Vernalis, Merck KGaA, and Sixth Element Capital outside the submitted work; and Chemical Probes Portal; P. Workman holds non-remunerated position of Executive Director in this nonprofit organization. A. Califano reports personal fees and other support from DarwinHealth Inc. outside the submitted work. M.M. Shen reports grants from NIH during the conduct of the study. A. Alimonti reports personal fees from IBSA International Sa; grants from IBSA International Sa, Novartis, AstraZeneca, Sun Pharma; and nonfinancial support from Oncosense outside the submitted work. W. Yuan reports Jilin Huarui Gene Technology supported travel grant. J. de Bono reports grants from Daiichi Sankyo during the conduct of the study; personal fees from Daiichi Sankyo, AstraZeneca, Genentech/Roche, Seagen, Novartis/AAA, GlaxoSmithKline, Pfizer, Amgen, Bayer, Janssen, and Astellas outside the submitted work. No disclosures were reported by the other authors.

Authors' Contributions

V. Gil: Conceptualization, data curation, formal analysis, validation, investigation, visualization, methodology, writing–original draft, writing–review and editing. **S. Miranda:** Conceptualization, data curation, formal analysis, validation,

investigation, visualization, methodology, writing–original draft, writing–review and editing. **R. Riisnaes:** Validation, methodology, writing–review and editing. **B. Gurel:** Data curation, formal analysis, writing–review and editing. **M. D'Ambrosio:** Investigation, methodology, writing–review and editing. **A. Vasciaveo:** Software, investigation, methodology, writing–review and editing. **M. Crespo:** Validation, methodology, writing–review and editing. **A. Ferreira:** Validation, methodology, writing–review and editing. **D. Brina:** Methodology, writing–review and editing. **M. Troiani:** Software, investigation, methodology, writing–review and editing. **A. Sharp:** Data curation, formal analysis, investigation, writing–original draft, writing–review and editing, patient selection and care for the overall study. **B. Sheehan:** Resources, writing–review and editing. **R. Christova:** Validation, methodology, writing–review and editing. **G. Seed:** Software, writing–review and editing. **I. Figueiredo:** Resources, writing–review and editing. **M. Lambros:** Resources, writing–review and editing. **D. Dolling:** Data curation, writing–review and editing. **J. Rekowski:** Data curation, formal analysis, writing–review and editing. **A. Alajati:** Resources, writing–review and editing. **M. Clarke:** Software, writing–review and editing. **R. Pereira:** Resources, writing–review and editing. **P. Flohr:** Resources, writing–review and editing. **G. Fowler:** Resources, writing–review and editing. **G. Boysen:** Resources, writing–review and editing. **S. Sumanasuriya:** Writing–review and editing, patient selection and care for the overall study. **D. Bianchini:** Resources, writing–review and editing, patient selection and care for the overall study. **P. Rescigno:** Resources, writing–review and editing, patient selection and care for the overall study. **C. Aversa:** Resources, writing–review and editing, patient selection and care for the overall study. **N. Tunariu:** Resources, writing–review and editing, patient selection and care for the overall study. **C. Guo:** Resources, writing–review and editing, patient selection and care for the overall study. **A. Paschalis:** Resources, writing–review and editing, patient selection and care for the overall study. **C. Bertan:** Methodology, writing–review and editing. **L. Buroni:** Validation, methodology, writing–review and editing. **J. Ning:** Resources, writing–review and editing. **S. Carreira:** Data curation, methodology, writing–review and editing. **P. Workman:** Supervision, writing–review and editing. **A. Swain:** Resources, writing–review and editing. **A. Califano:** Supervision, writing–review and editing. **M.M. Shen:** Supervision, writing–review and editing. **A. Alimonti:** Resources, supervision, writing–review and editing. **A. Neeb:** Resources, supervision, validation, methodology, writing–review and editing. **P. SU2C International Prostate Cancer Dream Team:** Writing–review and editing. **J. Welti:** Data curation, supervision, validation, investigation, visualization, methodology, writing–original draft, project administration, writing–review and editing. **W. Yuan:** Resources, data curation, software, formal analysis, supervision, investigation, visualization, methodology, project administration, writing–review and editing. **J. de Bono:** Conceptualization, resources, formal analysis, supervision, funding acquisition, investigation, writing–original draft, project administration, writing–review and editing.

Acknowledgments

Work in the de Bono laboratory was supported by funding from the Movember Foundation/Prostate Cancer UK (CEO13-2-002), the U.S. Department of Defense, the Prostate Cancer Foundation (20131017 and 20131017-1), Stand Up To Cancer (SU2C-AACR-DT0712), Cancer Research UK (CRM108X-A25144), and the UK Department of Health through an Experimental Cancer Medicine Centre grant (ECMC-CRM064X). Daiichi-Sankyo provided support for the generation of the IHC analyses for HER3, and donated U3-1402 and U3-1287. A. Vasciaveo is supported by the U.S. Department of Defense Early Investigator Research Award (W81XWH19-1-0337). G. Seed is currently supported by a post-doctoral fellowship from Prostate Cancer UK (TLD-PF19-005). A. Sharp has been supported by the Medical Research Council, the Academy of Medical Sciences, and Prostate Cancer UK, and is currently funded by the Prostate Cancer Foundation and Wellcome Trust. C. Guo is supported by grant funding from the Wellcome Trust, U.S. Department of Defense, and the Prostate Cancer Foundation. P. Workman was funded by Wellcome Trust, Chordoma Foundation, Mark Foundation for Cancer Research, and Cancer Research UK (including Cancer Research UK grants for the Cancer Therapeutic Unit at ICR and the Convergence Science Centre at ICR/Imperial) and he is a Cancer Research UK Life Fellow. A. Califano was supported by an NCI Outstanding Investigator Award (R35 CA197745). M.M. Shen is supported by NIH (R01 CA251527).

The costs of publication of this article were defrayed in part by the payment of page charges. This article must therefore be hereby marked *advertisement* in accordance with 18 U.S.C. Section 1734 solely to indicate this fact.

Received October 4, 2021; revised October 20, 2021; accepted October 25, 2021; published first November 9, 2021.

References

1. Sartor O, de Bono JS. Metastatic prostate cancer. N Engl J Med 2018;378:1653–4.
2. Armenia J, Wankowicz SAM, Liu D, Gao J, Kundra R, Reznik E, et al. The long tail of oncogenic drivers in prostate cancer. Nat Genet 2018;50:645–51.
3. Robinson D, Van Allen EM, Wu YM, Schultz N, Lonigro RJ, Mosquera JM, et al. Integrative clinical genomics of advanced prostate cancer. Cell 2015;162:454.
4. Sharp A, Coleman I, Yuan W, Sprenger C, Dolling D, Rodrigues DN, et al. Androgen receptor splice variant-7 expression emerges with castration resistance in prostate cancer. J Clin Invest 2019;129:192–208.
5. Einstein DJ, Arai S, Balk SP. Targeting the androgen receptor and overcoming resistance in prostate cancer. Curr Opin Oncol 2019;31:175–82.
6. Craft N, Shostak Y, Carey M, Sawyers CL. A mechanism for hormone-independent prostate cancer through modulation of androgen receptor signaling by the HER-2/neu tyrosine kinase. Nat Med 1999;5:280–5.
7. Molife LR, Omlin A, Jones RJ, Karavasilis V, Bloomfield D, Lumsden G, et al. Randomized Phase II trial of nintedanib, afatinib and sequential combination in castration-resistant prostate cancer. Future Oncol 2014;10:219–31.
8. de Bono JS, Bellmunt J, Attard G, Droz JP, Miller K, Flechon A, et al. Open-label phase II study evaluating the efficacy and safety of two doses of pertuzumab in castrate chemotherapy-naive patients with hormone-refractory prostate cancer. J Clin Oncol 2007;25:257–62.
9. Slamon D, Clark G, Wong S, Levin W, Ullrich A, McGuire W. Human breast cancer: correlation of relapse and survival with amplification of the HER-2/neu oncogene. Science 1987;235:177–82.
10. Koumakpayi IH, Diallo J-S, Le Page C, Lessard L, Gleave M, Bégin LR, et al. Expression and nuclear localization of ErbB3 in prostate cancer. Clin Cancer Res 2006;12:2730–7.
11. Masuda N, Yonemori K, Takahashi S, Kogawa T, Nakayama T, Iwase H, et al. Abstract PD1–03: single agent activity of U3–1402, a HER3-targeting antibody-drug conjugate, in HER3-overexpressing metastatic breast cancer: updated results of a phase 1/2 trial. Cancer Res 2019;79:PD1–03.
12. Poovassery JS, Kang JC, Kim D, Ober RJ, Ward ES. Antibody targeting of HER2/HER3 signaling overcomes heregulin-induced resistance to PI3K inhibition in prostate cancer. Int J Cancer 2015;137:267–77.
13. Tamura K, Tsurutani J, Takahashi S, Iwata H, Krop IE, Redfern C, et al. Trastuzumab deruxtecan (DS-8201a) in patients with advanced HER2-positive breast cancer previously treated with trastuzumab emtansine: a dose-expansion, phase 1 study. Lancet Oncol 2019;20:816–26.
14. Mateo J, Carreira S, Sandhu S, Miranda S, Mossop H, Perez-Lopez R, et al. DNA-repair defects and olaparib in metastatic prostate cancer. N Engl J Med 2015;373:1697–708.
15. Welti J, Sharp A, Brooks N, Yuan W, McNair C, Chand SN, et al. Targeting p300/CBP axis in lethal prostate cancer. Cancer Discov 2021;11:1118–37.
16. Welti J, Sharp A, Yuan W, Dolling D, Nava Rodrigues D, Figueiredo I, et al. Targeting bromodomain and extra-terminal (BET) family proteins in castration-resistant prostate cancer (CRPC). Clin Cancer Res 2018;24:3149–62.
17. Workman P, Aboagye EO, Balkwill F, Balmain A, Bruder G, Chaplin DJ, et al. Guidelines for the welfare and use of animals in cancer research. Br J Cancer 2010;102:1555–77.
18. Drost J, Karthaus WR, Gao D, Driehuis E, Sawyers CL, Chen Y, et al. Organoid culture systems for prostate epithelial and cancer tissue. Nat Protoc 2016;11:347–58.
19. Chen S, Zhu G, Yang Y, Wang F, Xiao YT, Zhang N, et al. Single-cell analysis reveals transcriptomic remodellings in distinct cell types that contribute to human prostate cancer progression. Nat Cell Biol 2021;23:87–98.
20. Wolf FA, Angerer P, Theis FJ. SCANPY: large-scale single-cell gene expression data analysis. Genome Biol 2018;19:15.

21. Polanski K, Young MD, Miao Z, Meyer KB, Teichmann SA, Park JE. BBKNN: fast batch alignment of single cell transcriptomes. Bioinformatics 2020;36: 964–5.
22. Traag VA, Waltman L, van Eck NJ. From Louvain to Leiden: guaranteeing well-connected communities. Sci Rep 2019;9:5233.
23. Aran D, Looney AP, Liu L, Wu E, Fong V, Hsu A, et al. Reference-based analysis of lung single-cell sequencing reveals a transitional profibrotic macrophage. Nat Immunol 2019;20:163–72.
24. Martens JH, Stunnenberg HG. BLUEPRINT: mapping human blood cell epigenomes. Haematologica 2013;98:1487–9.
25. de Souza N. The ENCODE project. Nat Methods 2012;9:1046.
26. McInnes L, Healy J, Melville J. Umap: uniform manifold approximation and projection for dimension reduction. arXiv preprint arXiv:180203426; 2018.
27. Becht E, McInnes L, Healy J, Dutertre CA, Kwok IWH, Ng LG, et al. Dimensionality reduction for visualizing single-cell data using UMAP. Nat Biotechnol 2018 [Online ahead of print].
28. Di Mitri D, Mirenda M, Vasilevska J, Calcinotto A, Delaleu N, Revandkar A, et al. Re-education of tumor-associated macrophages by CXCR2 blockade drives senescence and tumor inhibition in advanced prostate cancer. Cell Rep 2019; 28:2156–68.
29. Calcinotto A, Spataro C, Zagato E, Di Mitri D, Gil V, Crespo M, et al. IL-23 secreted by myeloid cells drives castration-resistant prostate cancer. Nature 2018;559:363–9.
30. Trapnell C, Roberts A, Goff L, Pertea G, Kim D, Kelley DR, et al. Differential gene and transcript expression analysis of RNA-seq experiments with TopHat and Cufflinks. Nat Protoc 2012;7:562–78.
31. Chen L, Siddiqui S, Bose S, Mooso B, Asuncion A, Bedolla RG, et al. Nrdp1-mediated regulation of ErbB3 expression by the androgen receptor in androgen-dependent but not castrate-resistant prostate cancer cells. Cancer Res 2010;70: 5994–6003.
32. Junttila TT, Akita RW, Parsons K, Fields C, Lewis Phillips GD, Friedman LS, et al. Ligand-independent HER2/HER3/PI3K complex is disrupted by trastuzumab and is effectively inhibited by the PI3K inhibitor GDC-0941. Cancer Cell 2009; 15:429–40.
33. Yarden Y, Sliwkowski MX. Untangling the ErbB signalling network. Nat Rev Mol Cell Biol 2001;2:127–37.
34. Carver Brett S, Chapinski C, Wongvipat J, Hieronymus H, Chen Y, Chandarlapaty S, et al. Reciprocal feedback regulation of PI3K and androgen receptor signaling in PTEN-deficient prostate cancer. Cancer Cell 2011;19: 575–86.
35. Mota JM, Collier KA, Barros Costa RL, Taxter T, Kalyan A, Leite CA, et al. A comprehensive review of heregulins, HER3, and HER4 as potential therapeutic targets in cancer. Oncotarget 2017;8:89284–306.
36. Zhang Z, Karthaus WR, Lee YS, Gao VR, Wu C, Russo JW, et al. Tumor microenvironment-derived NRG1 promotes antiandrogen resistance in prostate cancer. Cancer Cell 2020;38:279–96.
37. Ku SY, Rosario S, Wang Y, Mu P, Seshadri M, Goodrich ZW, et al. Rb1 and Trp53 cooperate to suppress prostate cancer lineage plasticity, metastasis, and antiandrogen resistance. Science 2017;355:78–83.
38. Yonesaka K, Takegawa N, Watanabe S, Haratani K, Kawakami H, Sakai K, et al. An HER3-targeting antibody-drug conjugate incorporating a DNA topoisomerase I inhibitor U3-1402 conquers EGFR tyrosine kinase inhibitor-resistant NSCLC. Oncogene 2019;38:1398–409.
39. Shimizu T, Yonesaka K, Hayashi H, Iwasa T, Haratani K, Yamada H, et al. Phase 1 study of new formulation of patritumab (U3-1287) Process 2, a fully human anti-HER3 monoclonal antibody in combination with erlotinib in Japanese patients with advanced non-small cell lung cancer. Cancer Chemother Pharmacol 2017;79:489–95.
40. Hashimoto Y, Koyama K, Kamai Y, Hirotani K, Ogitani Y, Zembutsu A, et al. A novel HER3-targeting antibody–drug conjugate, U3-1402, exhibits potent therapeutic efficacy through the delivery of cytotoxic payload by efficient internalization. Clin Cancer Res 2019;25:7151–61.
41. Yap TA, Smith AD, Ferraldeschi R, Al-Lazikani B, Workman P, de Bono JS. Drug discovery in advanced prostate cancer: translating biology into therapy. Nat Rev Drug Discov 2016;15:699–718.
42. de Bono JS, Logothetis CJ, Molina A, Fizazi K, North S, Chu L, et al. Abiraterone and increased survival in metastatic prostate cancer. N Engl J Med 2011;364: 1995–2005.
43. Xie T, Lim SM, Westover KD, Dodge ME, Ercan D, Ficarro SB, et al. Pharmacological targeting of the pseudokinase Her3. Nat Chem Biol 2014;10:1006–12.
44. Shi F, Telesco SE, Liu Y, Radhakrishnan R, Lemmon MA. ErbB3/HER3 intracellular domain is competent to bind ATP and catalyze autophosphorylation. Proc Natl Acad Sci U S A 2010;107:7692–7.
45. Li C, Wang S, Xing Z, Lin A, Liang K, Song J, et al. A ROR1-HER3-lncRNA signalling axis modulates the Hippo-YAP pathway to regulate bone metastasis. Nat Cell Biol 2017;19:106–19.
46. Hsieh AC, Moasser MM. Targeting HER proteins in cancer therapy and the role of the non-target HER3. Br J Cancer 2007;97:453–7.
47. Ptakova N, Martinek P, Holubec L, Janovsky V, Vancurova J, Grossmann P, et al. Identification of tumors with NRG1 rearrangement, including a novel putative pathogenic UNC5D-NRG1 gene fusion in prostate cancer by data-drilling a de-identified tumor database. Genes Chromosomes Cancer 2021;60:474–81.
48. Puca L, Bareja R, Prandi D, Shaw R, Benelli M, Karthaus WR, et al. Patient derived organoids to model rare prostate cancer phenotypes. Nat Commun 2018;9:2404.
49. Revandkar A, Perciato ML, Toso A, Alajati A, Chen J, Gerber H, et al. Inhibition of Notch pathway arrests PTEN-deficient advanced prostate cancer by triggering p27-driven cellular senescence. Nat Commun 2016;7:13719.

Published OnlineFirst November 9, 2021; DOI: 10.1158/0008-5472.CAN-21-3360

Cancer Research
The Journal of Cancer Research (1916–1930) | The American Journal of Cancer (1931–1940)

AACR American Association for Cancer Research

HER3 Is an Actionable Target in Advanced Prostate Cancer

Veronica Gil, Susana Miranda, Ruth Riisnaes, et al.

Cancer Res 2021;81:6207-6218. Published OnlineFirst November 9, 2021.